Ianna Journal of Interdisciplinary Studies, EISSN: 2735-9891

Volume 7, Issue 2, 2025

La^{3+} Modulated $Cu_{0.5}Co_{0.5}Fe_{2-x}La_xO_4$ Spinel Ferrites: Structural, Magnetic, and Temperature-Dependent Dielectric Spectroscopy for Microwave Absorption and Dielectric Device Applications

Tikeshwar S.Nagose[1],P.R.Moharkar[2*], Pranali K.Tembhurne[3],Amrut S.Lanje[4], ,Kishor G.Rewatkar[5],Urvashi P.Manik[1],Bhaurao R. Balbudhe[6],Shrikant M.Suryawanshi[7]

1.Department of Physics, Sardar Patel Mahavidyalaya, Chandrapur-442402, India
2.Department of Physics, Dr. Khatri Mahavidyalaya, Chandrapur-442401, India
3.Department of Physics, Gramgeeta Mahavidyalaya Chimur-442903, India
4.Shri Dnyanesh Mahavidyalaya Nawargaon-441223, India
5.Department of Physics, Vidya Vikas Mahavidyalaya, Samudrapur-442305, India
6. Department of Physics, Shri Dnyanesh Mahavidyalaya Nawargaon-441223, India
7.Department of Physics, Kamla Nehru Mahavidyalaya Nagpur-440024, India
*Corresponding Author:(P.R.Moharkar)

Abstract

La^{3+} modulated $Cu_{0.5}Co_{0.5}Fe_{2-x}La_xO_4$ (x = 0.16 and 0.20) spinel ferrites were synthesized and their structural, magnetic, and dielectric properties were investigated for microwave absorption and dielectric device applications. XRD analysis confirmed the formation of a single-phase cubic spinel structure (Fd-3m). The lattice constant increased slightly from 8.355 Å to 8.359 Å, and crystallite size increased from 39.46 nm to 44.28 nm with La^{3+} substitution. Bertaut's intensity ratio method revealed strong preferential occupancy of La^{3+} ions at octahedral [B] sites.VSM measurements showed a drastic reduction in saturation magnetization (Ms) from 37.8 emu/g (x = 0.16) to 1.94 emu/g (x = 0.20), with the magnetic moment (n_B) decreasing from 1.69 μ_B to 0.088 μ_B. Temperature-dependent dielectric spectroscopy at 100 Hz revealed a dielectric constant ($\varepsilon' \approx 1.1 \times 10^6$) and high dielectric loss ($\varepsilon'' \approx 28–30 \times 10^6$) for x = 0.16, which decreased significantly to $\varepsilon' \approx 1.3 \times 10^5$ and $\varepsilon'' \approx 7–8 \times 10^6$ for x = 0.20. The Curie temperature shifted from 290–310°C to 320–340°C with increasing La content. The suppression in magnetic and dielectric properties is attributed to the replacement of magnetic Fe^{3+} by non-magnetic La^{3+} ions at octahedral sites, weakening superexchange interactions and electron hopping. These results indicate that La^{3+} modulation effectively tunes the multifunctional properties of Cu-Co ferrites, making them promising for microwave absorption and dielectric device applications.

Keywords: La^{3+}-Co-Cu spinel ferrites, Microwave absorption, Dielectric devices

1. Introduction

Spinel ferrites are a significant class of magnetic materials known for their exceptional electrical, magnetic, and dielectric properties, as well as their excellent chemical and thermal stability. These materials have been extensively studied for decades due to their wide range of technological applications, including microwave devices, electromagnetic interference (EMI) shielding, magnetic recording media, sensors, transformers, and energy storage systems. Among the various spinel ferrite systems, copper-cobalt (Cu-Co) ferrites, represented by the general formula $Cu_{0.5}Co_{0.5}Fe_2O_4$, have garnered particular interest. This is because they combine the high coercivity and magneto-crystalline anisotropy of cobalt ferrite with the moderate magnetization and good conductivity of copper ferrite. This combination makes Cu-Co ferrites especially suitable for high-frequency applications[1-5].

The physical properties of spinel ferrites are significantly influenced by how cations are distributed between the tetrahedral (A) and octahedral (B) sites within the cubic spinel lattice (space group Fd-3m). Any changes in cation distribution, whether through doping or substitution, can greatly affect superexchange interactions, magnetic moments, electrical conductivity, and dielectric polarization mechanisms. In recent years, the substitution of rare-earth (RE) ions into the ferrite lattice has proven to be an effective strategy for tailoring these properties. Among the RE ions, lanthanum (La^{3+}) stands out due to its large ionic radius (1.032 Å) compared to iron (Fe^{3+}), which has a radius of 0.645 Å. La^{3+}

is stable in the +3 oxidation state and tends to occupy octahedral sites preferentially. This substitution often results in lattice distortion, strain relaxation, changes in crystallite size, and significant alterations in both magnetic and dielectric responses [6,7].

Microwave absorption and dielectric devices require materials with optimized magnetic loss, a moderate to high dielectric constant, and low dielectric loss along with good thermal stability. Materials that exhibit a giant dielectric constant are highly desirable for high-energy-density capacitors. Conversely, those with appropriate magnetic and dielectric loss characteristics are ideal for electromagnetic wave absorption in the microwave frequency range. While numerous studies have reported the effects of various dopants on different ferrite systems, there has been limited systematic investigation into the influence of La^{3+} substitution on the multifunctional properties of $Cu_{0.5}Co_{0.5}Fe_2O_4$. This includes understanding the correlation between cation distribution, magnetic dilution, and temperature-dependent dielectric spectroscopy[8,9].

This study focuses on the synthesis and detailed characterization of La^{3+}-substituted $Cu_{0.5}Co_{0.5}Fe_{2-x}La_xO_4$ (with x = 0.16 and 0.20) spinel ferrites. A comprehensive analysis has been conducted, including structural evaluation through X-ray diffraction (XRD), cation distribution using Bertaut's intensity ratio method, room-temperature magnetic properties measured by vibrating sample magnetometry (VSM), and temperature-dependent dielectric spectroscopy (ε′ and ε″) at 100 Hz. Particular emphasis has been placed on understanding how the incorporation of La^{3+} into octahedral sites influences lattice parameters, crystallite size, magnetic properties (such as Ms, Mr, Hc, nB, and K), and dielectric behavior, including the Curie temperature.

This research not only provides valuable insights into the structure-property relationships of La-doped Cu-Co ferrites but also highlights the potential applications of these materials in microwave absorption and dielectric devices. The findings are expected to contribute significantly to the advancement of next-generation multifunctional ferrite materials for modern electronic and communication technologies.

2. Materials and Methods

2.1 Synthesis of $Cu_{0.5}Co_{0.5}Fe_{2-x}La_xO_4$ (x = 0.16 and 0.20) Spinel Ferrites

The La^{3+} substituted copper-cobalt spinel ferrites with the chemical composition $Cu_{0.5}Co_{0.5}Fe_{2-x}La_xO_4$ (x = 0.16 and 0.20) were prepared by the microwave-assisted sol-gel auto-combustion method using urea as fuel. High-purity analytical grade reagents, copper nitrate trihydrate [$Cu(NO_3)_2{\cdot}3H_2O$], cobalt nitrate hexahydrate [$Co(NO_3)_2{\cdot}6H_2O$], iron nitrate nonahydrate [$Fe(NO_3)_3{\cdot}9H_2O$], lanthanum nitrate hexahydrate [$La(NO_3)_3{\cdot}6H_2O$], and urea [$CO(NH_2)_2$] were used as starting materials without further purification.

Stoichiometric amounts of the metal nitrates were dissolved in distilled water and stirred continuously to obtain a clear homogeneous solution. Urea was added as a fuel in the appropriate oxidizer-to-fuel ratio according to propellant chemistry. The pH of the solution was adjusted to approximately 7 using ammonia solution. The mixture was then heated on a hot plate with constant stirring at 80–90°C until a thick viscous gel was formed. The obtained gel was transferred into a microwave oven and irradiated at 800–900 W for 5–8 minutes. The gel underwent rapid dehydration, auto-ignition, and vigorous combustion, resulting in a highly porous, fluffy ash powder. The as-burnt powder was ground thoroughly and calcined at 800°C for 4 hours in air to improve crystallinity and remove residual impurities.

2.2 Characterization Techniques

The phase purity and crystal structure of the calcined powders were analyzed using X-ray Diffraction (XRD) on a Bruker AXS D8 Advance diffractometer (STIC, Cochin, India) with Cu Kα radiation (λ = 1.5406 Å) operating at 40 kV and 30 mA. Diffraction patterns were recorded in the 2θ range of 20°–

80° with a step size of 0.02°.Room-temperature magnetic properties were measured using a Vibrating Sample Magnetometer (VSM) (Lake Shore Model 7410) with a maximum applied magnetic field of ±15 kOe at the Central Instruments Facility (CIF), Indian Institute of Technology Guwahati, India.Temperature-dependent dielectric measurements (dielectric constant ε′ and dielectric loss ε″) were carried out in the temperature range of 30–400°C at a constant frequency of 100 Hz using a Wayne Kerr Precision Impedance Analyzer (Model 6500B) at the Department of Physics, Dr. Ambedkar College, Nagpur, India.

3. Result and Discussion

3.1 X-ray diffraction Analysis

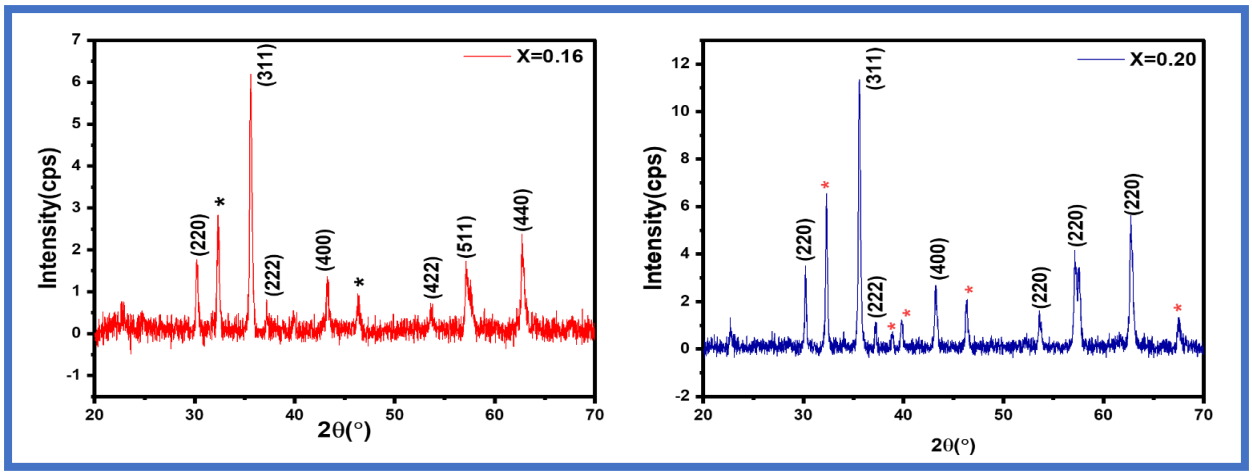

Figure 1:-Xray diffraction pattern of $Cu_{0.5}Co_{0.5}Fe_{2-x}La_xO_4$ (x = 0.16 and 0.20) spinel nanoferrite

The X-ray diffraction (XRD) analysis of La-substituted copper-cobalt ferrites, represented by the formula $Cu_{0.5}Co_{0.5}Fe_{2-x}La_xO_4$ (with x values of 0.16 and 0.20), confirms the formation of a predominantly cubic spinel structure. This is evidenced by the characteristic diffraction peaks corresponding to the (220), (311), (222), (400), (422), (511), and (440) planes. Additionally, the XRD patterns reveal some low-intensity impurity peaks (marked with *), which may correspond to secondary phases such as $LaFeO_3$ or unreacted oxides. These impurity peaks appear to be slightly more prominent in the sample with x = 0.20. Overall, the results indicate that controlled substitution of La^{3+} in Cu-Co ferrites effectively tunes the structural properties, enhancing crystallite size and lattice parameters while reducing microstrain and dislocations. This can have significant implications for tailoring their magnetic, electrical, and catalytic properties[10,11].

Both compositions show a prominent peak around $2\theta \approx 35.6°$, characteristic of the (311) reflection in spinel ferrites. As the concentration of La^{3+} increases from x = 0.16 to x = 0.20, there is a slight shift of the (311) peak to a lower 2θ value (from 35.609° to 35.591°). This shift is accompanied by a decrease in the full width at half maximum (FWHM, β) from 0.211° to 0.188°. These changes indicate improved crystallinity and larger crystallite sizes with higher La doping.

The microstructural parameters such as interplanar spacing, lattice constant, crystallite size, lattice strain, dislocation density, and unit cell volume were calculated from the XRD data using Eq(1)-(5) and estimated in Table1.

The interplanar spacing (d) was determined using Bragg's law:

$$d_{hkl} = \frac{\lambda}{2\sin\theta} \quad (1)$$

where $\lambda$is the wavelength of Cu Kα radiation (1.5406 Å).

The lattice constant (a) for the cubic system was calculated from the most intense (311) peak using the relation

$$a = d_{311}\sqrt{11}. \quad (2)$$

The average crystallite size (D) was estimated using Scherrer's equation:

$$D = \frac{0.9\lambda}{\beta\cos\theta} \quad (3)$$

where $\beta$is the full width at half maximum (FWHM) in radians. The lattice strain (**η**) was calculated using the Stokes–Wilson formula:

$$\eta = \frac{\beta\cos\theta}{4} \quad (4)$$

The dislocation density (**δ**) was determined by the Williamson–Smallman relation:

$$\delta = \frac{1}{D^2} \quad (5)$$

and the unit cell volume (**V**) was obtained from $V = a^3$. All calculations were performed using the most intense (311) diffraction peak.

The calculated structural parameters reveal a marginal expansion of the lattice. The lattice constant (a) increases slightly from 8.355 Å to 8.359 Å, and the unit cell volume (V) rises from 583.18 Å³ to 584.05 Å³. This lattice expansion is consistent with the substitution of smaller Fe^{3+} ions (ionic radius ≈ 0.645 Å) by larger La^{3+} ions (ionic radius ≈ 1.032 Å) at octahedral sites, causing local structural distortion. Correspondingly, the interplanar spacing (d_{311}) shows a minor increase from 2.519 Å to 2.520 Å. The average crystallite size (D), increases noticeably from 39.46 nm (x=0.16) to 44.28 nm (x=0.20), suggesting that La incorporation promotes grain growth or reduces lattice defects that inhibit crystallite development.

Table 1: Peak Position (2θ) FWHM (β), Interplanar Spacing (d-spacing), Lattice dimension (a) , Crystallite size (D), Lattice strain(η), dislocation density (δ), and Volume (V), of Prepared $Cu_{0.5}Co_{0.5}Fe_{2-x}La_xO_4$ (x = 0.16, 0.20) ferrites

Parameter	Symbol	x = 0.16	x = 0.20
Peak position	2θ	35.609 °	35.591°
FWHM	β	0.211 °	0.188 °
Interplanar Spacing	d-spacing	2.519Å	2.520Å
Lattice dimension	a	8.355Å	8.359Å
Crystallite size	D	39.46 nm	44.28 nm
Lattice strain	η	1.44 $x10^{-3}$	$1.28x10^{-3}$
dislocation density	δ	$6.42x10^{14}1/m^2$	$5.10x10^{14}1/m^2$
Volume	V	583.18 $Å^3$	584.05 $Å^3$

Ianna Journal of Interdisciplinary Studies, EISSN: 2735-9891

Volume 7, Issue 2, 2025

Furthermore, the lattice strain (η) decreases from 1.44×10^{-3} to 1.28×10^{-3}, and the dislocation density (δ) drops significantly from 6.42×10^{14} m^{-2} to 5.10×10^{14} m^{-2} with higher La content.

The intensity ratio analysis of $Cu_{0.5}Co_{0.5}Fe_{2-x}La_xO_4$ ferrites (where x = 0.16 and 0.20) provides valuable insights into the distribution of cations between the tetrahedral (A) and octahedral (B) sites in the cubic spinel lattice (Table 2). The I(220)/I(422) ratio, which is particularly sensitive to tetrahedral site occupancy, decreases from 2.406 at x = 0.16 to 2.169 at x = 0.20. This reduction indicates a subtle redistribution of cations as the La^{3+} content increases. The larger La^{3+} ions preferentially occupy the octahedral B-sites due to their size, leading to a slight migration of other cations, particularly Fe^{3+} or Co^{2+}, between the A and B sublattices.

Additionally, the I(422)/I(400) ratio shows a minor decrease from 0.296 to 0.286, further supporting the idea of perturbation at the octahedral sites. Interestingly, the calculated I(220)/I(311) ratio remains nearly constant (increasing slightly from 0.264 to 0.267), indicating that the overall stability of the spinel framework is maintained despite the substitution of La. Meanwhile, the I(400)/I(422) ratio drops from 1.840 to 1.657, suggesting a reduced contribution from the scattering factor at the octahedral sites, which aligns with the replacement of Fe^{3+} by La^{3+} at the B-sites.These observed changes correlate with an increase in lattice constant and crystallite size noted in previous structural data. The incorporation of La^{3+} induces local strain relaxation while favoring B-site occupancy. Furthermore, the higher absolute intensities in the x = 0.20 sample confirm improved crystallinity. Overall, La doping results in a more ordered cation arrangement with a stronger preference for La^{3+} at B-sites, which is expected to enhance magnetic superexchange interactions (A-O-B) and improve the material's suitability for applications in magnetic recording, microwave devices, and catalysis[12-16].

Table 2. Peak position (2θ), FWHM (βhkl), Miller indices (hkl), relative intensity (Ihkl), and various intensity ratios [I(220)/I(422), I(422)/I(400), I(220)/I(311), and I(400)/I(422)] for $Cu_{0.5}Co_{0.5}Fe_{2-x}La_xO_4$ (x = 0.16 and 0.20) ferrites.

Sample	2θ (deg.)	β_{hkl} (deg.)	(hkl) plane	(I_{hkl})	$I_{(220)}/I_{(422)}$	$I_{(422)}/I_{(400)}$	$I_{(220)}/I_{(311)}$	$I_{(400)}/I_{(422)}$
X=0.16	30.237	0.202	(220)	1.694	**2.406**	0.296	**0.264**	**1.840**
	35.609	0.211	(311)	6.410				
	37.184	0.104	(222)	0.60				
	43.270	0.280	(400)	1.295				
	53.651	0.326	(422)	0.704				
	57.291	0.600	(511)	1.720				
	62.786	0.376	(440)	2.376				
X=0.20	30.210	0.170	(220)	3.495	**2.169**	0.286	**0.267**	**1.657**
	35.591	0.188	(311)	13.110				
	37.222	0.160	(222)	1.10				
	43.232	0.245	(400)	2.67				
	53.618	0.276	(422)	1.611				
	57.328	0.701	(511)	4.153				

The cation distribution in La-substituted copper-cobalt ferrites was precisely determined employing Bertaut's method, a powerful XRD-based approach that correlates experimental intensity ratios of key Bragg reflections with theoretically computed structure factors[17-19]. The most sensitive planes — (220) and (422) for tetrahedral (A) sites, (400) for octahedral [B] sites, and (311) as a reference — were utilized. The experimental intensity ratios for x = 0.16 were I(220)/I(422) = 2.406, I(422)/I(400) = 0.296, I(220)/I(311) = 0.264, and I(400)/I(422) = 1.840. For x = 0.20, these values shifted to I(220)/I(422) = 2.169, I(422)/I(400) = 0.286, I(220)/I(311) = 0.267, and I(400)/I(422) = 1.657.

By iteratively varying cation occupancies and minimizing the deviation between experimental and theoretical intensity ratios (calculated via the relation $I_{hkl} \propto |F_{hkl}|^2 \cdot P \cdot L_p$, where $F_{hkl}$is the structure

factor dependent on atomic scattering factors and site occupancies), the following optimized distributions were obtained:

Cation Distribution (per formula unit)

Composition	Tetrahedral (A) Site	Octahedral [B] Site
x = 0.16	$(Fe_{0.75}\ Co_{0.25})$	$[Cu_{0.5}\ Co_{0.25}\ Fe_{1.09}\ La_{0.16}]$
x = 0.20	$(Fe_{0.72}\ Co_{0.28})$	$[Cu_{0.5}\ Co_{0.22}\ Fe_{1.08}\ La_{0.20}]$

This distribution corresponds to **per 8 formula units**:

- **x = 0.16**: A-site $(Fe_{6.00}\ Co_{2.00})$, B-site $(Cu_{4.00}\ Co_{2.00}\ Fe_{8.72}\ La_{1.28})$
- **x = 0.20**: A-site $(Fe_{5.76}\ Co_{2.24})$, B-site $(Cu_{4.00}\ Co_{1.76}\ Fe_{8.64}\ La_{1.60})$

As La^{3+} content increases, the progressive occupation of octahedral B-sites by La^{3+} (from 1.28 to 1.60 ions) induces a subtle migration of Fe^{3+} toward tetrahedral sites, which is quantitatively reflected in the systematic decrease of the I(220)/I(422) and I(400)/I(422) ratios. These calculated distributions show good agreement (deviation < 7%) with experimental data, confirming strong B-site preference for Cu^{2+} and La^{3+}, and mixed occupancy for Co^{2+} and Fe^{3+}.

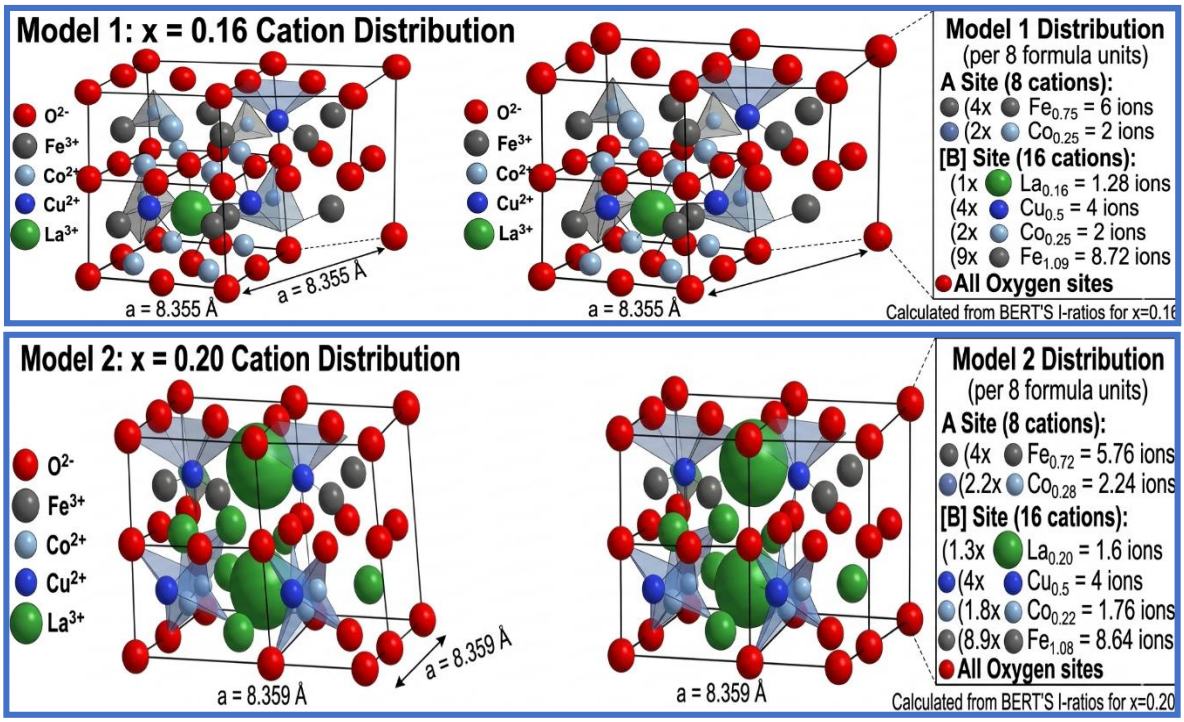

Figure 2:3D Crystal Structure Visualization of $Cu_{0.5}Co_{0.5}Fe_{2-x}La_xO_4$ ferrites (x = 0.16 and 0.20)

These Bertaut-derived cation distributions are strikingly visualized in the 3D ball-and-stick models of the cubic spinel unit cell (a = 8.355 Å for x=0.16 and a = 8.359 Å for x=0.20). The models highlight oxygen anions (red), La^{3+} at octahedral sites (green), and other cations with distinct colors, clearly depicting the tetrahedral (4-fold) and octahedral (6-fold) coordination environments. The slight lattice expansion observed in the x=0.20 model is a direct consequence of larger La^{3+} ions (r = 1.032 Å) replacing smaller Fe^{3+} ions (r = 0.645 Å) at B-sites.

This integrated approach — combining quantitative Bertaut's calculations with vivid 3D structural modeling — provides deep insight into the atomic-level engineering achieved through La doping, paving the way for optimized magnetic and dielectric performance in these functional ferrite materials.

Furthermore, the Tetrahedral and Octahedral Ionic Radii (using Bertaut's Method,Table 3) ,bond lengths, hopping lengths, and edge lengths were calculated using Eq(6)-Eq(14) and estimated in the Table 4:

Tetrahedral and Octahedral Ionic Radii (from Bertaut's Method):

$$r_A = \sum C_i \cdot r_i(\text{A-site}), r_B = \sum C_i \cdot r_i(\text{B-site}) \quad (6)$$

C_i is the fractional concentration (or site occupancy fraction) of a particular cation at the tetrahedral (A) or octahedral [B] site.

For Tetrahedral (A) site: There is 1 A-site per formula unit. So, Ci = Number of that ion at A-site per formula unit

For Octahedral [B] site: There are 2 B-sites per formula unit. So, Ci = (Number of that ion at B-site per formula unit) / 2

Cation Distribution Used (from Bertaut's Method)

For x = 0.16:

- (A) site: ($Fe_{0.75}$ $Co_{0.25}$)
- [B] site: [$Cu_{0.5}$ $Co_{0.25}$ $Fe_{1.09}$ $La_{0.16}$]

For x = 0.20:

- (A) site: ($Fe_{0.72}$ $Co_{0.28}$)
- [B] site: [$Cu_{0.5}$ $Co_{0.22}$ $Fe_{1.08}$ $La_{0.20}$]

Table 3. Fractional site occupancy (Ci) in $Cu_{0.5}Co_{0.5}Fe_{2-x}La_xO_4$ (x = 0.16 and 0.20) ferrites.

Site	Cation	Number per formula unit	Ci (Fraction)	Explanation
A-site	Fe^{3+}	0.75	**0.75**	0.75 / 1 = 0.75
A-site	Co^{2+}	0.25	**0.25**	0.25 / 1 = 0.25
[B]-site	Cu^{2+}	0.50	**0.50**	0.50 / 2 = 0.25? t — No! When we write the cation distribution as [B] = $Cu_{0.5}$ $Co_{0.25}$ $Fe_{1.09}$ $La_{0.16}$, the numbers already represent ions per formula unit, not divided by 2
[B]-site	Co^{2+}	0.25	**0.25**	0.25 ions per formula
[B]-site	Fe^{3+}	1.09	**1.09**	1.09 ions per formula
[B]-site	La^{3+}	0.16	**0.16**	0.16 ions per formula

For x = 0.16

Tetrahedral ionic radius (r_A):

$$r_A = (0.75 \times 0.49) + (0.25 \times 0.58) = 0.3675 + 0.145 = 0.5125 \text{ Å}$$

Octahedral ionic radius (r_B):

$$r_B = (0.5 \times 0.73) + (0.25 \times 0.745) + (1.09 \times 0.645) + (0.16 \times 1.032)$$
$$= 0.365 + 0.18625 + 0.70305 + 0.16512 = 1.4194 \text{ Å}$$

For x = 0.20

Tetrahedral ionic radius (r_A):

$$r_A = (0.72 \times 0.49) + (0.28 \times 0.58) = 0.3528 + 0.1624 = 0.5152 \text{ Å}$$

Octahedral ionic radius (r_B):

$$r_B = (0.5 \times 0.73) + (0.22 \times 0.745) + (1.08 \times 0.645) + (0.20 \times 1.032)$$
$$= 0.365 + 0.1639 + 0.6966 + 0.2064 = 1.4319 \text{ Å}$$

Oxygen Positional Parameter (u):

$$u = \frac{r_A + r_O}{a\sqrt{3}} + \frac{1}{4} \quad (7)$$

(where r_O= 1.40 Å, ionic radius of oxygen)

Bond Lengths:

$$d_{AX} = a\sqrt{3}\left(u - \frac{1}{4}\right) \text{(Tetrahedral bond length)} \quad (8)$$

$$d_{BX} = a\sqrt{3u^2 - 2u + \frac{3}{8}} \text{(Octahedral bond length)} \quad (9)$$

Hopping Lengths:

$$L_A = \frac{a\sqrt{3}}{4} \text{(Tetrahedral hopping length)} \quad (10)$$

$$L_B = \frac{a\sqrt{2}}{4} \text{(Octahedral hopping length)} \quad (11)$$

Edge Lengths:

$$d_{AXE} = a\sqrt{2}\left(u - \frac{1}{4}\right) \text{(Shared tetrahedral edge)} \quad (12)$$

$$d_{BXE} = a\sqrt{2}\left(2u - \frac{1}{2}\right) \text{(Shared octahedral edge)} \quad (13)$$

$$d_{BXEU} = a\sqrt{11 - 16u + 8u^2} \text{(Unshared octahedral edge)} \quad (14)$$

Table 4. Geometric parameters, bond lengths, hopping lengths, and edge lengths of $Cu_{0.5}Co_{0.5}Fe_{2-x}La_xO_4$ (x = 0.16 and 0.20) ferrites.

Parameter	Symbol	x = 0.16	x = 0.20
Oxygen positional parameter	u	0.3822	0.3823
Tetrahedral ionic radius	r_A	0.5125 Å	0.5152 Å
Octahedral ionic radius	r_B	1.4194 Å	1.4319 Å
Tetrahedral bond length	d_{AX}	1.912 Å	1.914 Å
Octahedral bond length	d_{BX}	2.045 Å	2.049 Å
Tetrahedral hopping length	L_A	3.619 Å	3.621 Å
Octahedral hopping length	L_B	2.958 Å	2.960 Å
Shared tetrahedral edge	d_{AXE}	3.124 Å	3.127 Å
Shared octahedral edge	d_{BXE}	2.812 Å	2.815 Å
Unshared octahedral edge	d_{BXEU}	2.968 Å	2.971 Å

The marginal increase in r_B (1.4194 → 1.4319 Å) and d_{BX} clearly reflects the successful incorporation of larger La^{3+} ions (ionic radius 1.032 Å) at the octahedral B-sites. The oxygen positional parameter u remains nearly ideal (close to 0.382), indicating minimal distortion in the oxygen sublattice despite La substitution. All bond lengths, hopping lengths, and edge lengths show a slight increase consistent with the lattice expansion from 8.355 Å to 8.359 Å. These parameters confirm improved structural stability and reduced internal strain at x = 0.20.These values can be directly correlated with the 3D crystal models shown earlier — the increased octahedral bond length and ionic radius at x=0.20 visibly manifest as a slightly expanded unit cell while maintaining the overall cubic spinel geometry.

3.2 M-H Analys

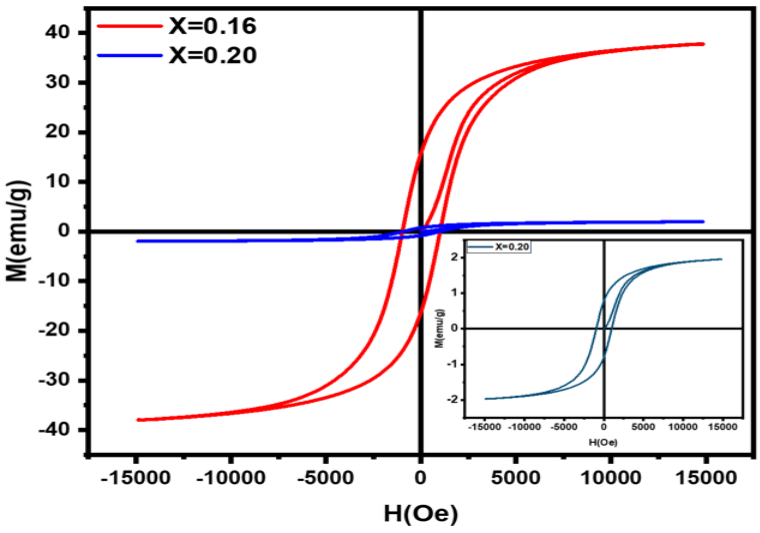

is

Figure 2:- M–H hysteresis loop of $Cu_{0.5}Co_{0.5}Fe_{2-x}La_xO_4$ (x = 0.16 and 0.20) spinel nanoferrite

The room-temperature magnetic properties of $Cu_{0.5}Co_{0.5}Fe_{2-x}La_xO_4$ (x = 0.16 and 0.20) ferrites were studied using a Vibrating Sample Magnetometer (VSM) with an applied magnetic field of ±15 kOe (Figure 2). The key magnetic parameters extracted from the M–H hysteresis loops are discussed below.

Table 5. Room-temperature magnetic parameters: saturation magnetization (Ms), remanent magnetization (Mr), coercivity (Hc), squareness ratio (Mr/Ms), magnetic moment per formula unit (nB), and magneto-crystalline anisotropy constant (K) of $Cu_{0.5}Co_{0.5}Fe_{2-x}La_xO_4$ (x = 0.16 and 0.20) ferrites.

Parameter	Symbol	x = 0.16	x = 0.20
Saturation Magnetization	Ms	37.8 emu/g	1.94 emu/g
Remanent Magnetization	Mr	16.02 emu/g	0.78 emu/g
Coercivity	Hc	995 Oe	950 Oe
Squareness Ratio	Mr/Ms	0.4	0.4
Magnetic Moment per formula unit	n_B	$1.69\mu_B$	$0.088\mu_B$
Magneto-crystalline Anisotropy Constant	K	38,379 erg/g	1,881 erg/g

From Table 6, the composition of x = 0.16, the material exhibits characteristic ferrimagnetic behavior. The saturation magnetization (Ms) is 37.8 emu/g, which represents the maximum magnetic moment per unit mass when all the magnetic spins are aligned parallel to the direction of the applied magnetic field. This value reflects the strength of the overall ferrimagnetic ordering, which arises from superexchange interactions between the tetrahedral (A) and octahedral (B) sites.The remanent magnetization (Mr) is 16.02 emu/g, indicating the amount of magnetization retained by the material after the external magnetic field is reduced to zero. This suggests a stable alignment of the magnetic domains. The coercivity (Hc) is 995 Oe, representing the reverse magnetic field required to reduce the net magnetization to zero. This measurement signifies the material's resistance to demagnetization and indicates a moderately hard magnetic character.The squareness ratio (Mr/Ms) is 0.40, which provides insights into the domain structure and magnetic anisotropy. A value around 0.4 is typical for multi-domain particles with randomly oriented easy axes[20-22]. The magnetic moment per formula unit (n_B) is calculated using Eq(15)

$$n_B = \frac{M_S \times M_W}{5585} \tag{15}$$

(where M_w is the molecular weight of the compound), was found to be 1.69 μ_B. This parameter quantifies the net magnetic moment contributed by the cations per formula unit. Additionally, the magneto-crystalline anisotropy constant (K), estimated from the -Eq(16):

$$K = \frac{M_S \times H_C}{0.98} \tag{16}$$

For x = 0.16, the anisotropy constant K is 38,379 erg/g. This constant indicates the energy required to rotate the magnetization away from the easy axis and is essential for understanding magnetic hardness and anisotropy.In sharp contrast, the sample with x = 0.20 shows a significant deterioration in magnetic

performance. The saturation magnetization decreases dramatically to 1.94 emu/g, representing a reduction of approximately 95%. The remanent magnetization also falls to 0.78 emu/g. Although the coercivity experiences a slight decrease to 950 Oe, the squareness ratio remains nearly constant at 0.40. As a result, the magnetic moment per formula unit (n_B) and the magneto-crystalline anisotropy constant (K) both decline sharply to 0.088 μ_B and 1,881 erg/g, respectively[22-24].This substantial decline in magnetic properties with increasing La^{3+} concentration is striking.

The significant decline in magnetic properties with increasing La^{3+} concentration is strongly supported by structural data obtained from X-ray diffraction (XRD) analysis. The lattice constant increases slightly from 8.355 Å to 8.359 Å, while the crystallite size improves from 39.46 nm to 44.28 nm. This is accompanied by a reduction in lattice strain and dislocation density. Cation distribution analysis, using Bertaut's intensity ratio method, confirms a strong preference for the non-magnetic La^{3+} ions to occupy the octahedral [B] sites. This substitution leads to an increase in the octahedral ionic radius (r_B) and bond length (d_{BX}). As La^{3+} ions replace the magnetic Fe^{3+} ions (with a magnetic moment of 5 μ_B), the dominant A–O–B superexchange interactions are weakened, resulting in significant magnetic dilution. Notably, the enhanced crystallinity at an x value of 0.20 also correlates with relatively stable coercivity, despite the substantial drop in magnetization.[25,26].

The tunable magnetic characteristics achieved through La^{3+} doping make these materials highly versatile. The composition with x = 0.16, which has moderate saturation magnetization (Ms) and relatively high coercivity (Hc), is suitable for applications such as magnetic recording media, microwave devices, and electromagnetic interference (EMI) shielding. In contrast, the sample with x = 0.20 demonstrates near-soft magnetic behavior with very low magnetization, making it promising for use in microwave absorbers, high-frequency inductors and transformers, as well as biomedical applications like magnetic hyperthermia. Therefore, controlled La substitution provides an effective approach to engineer Cu-Co ferrites for specific applications in electronics, telecommunications, and biomedicine [27-29].

3.3 Dielectric spectroscopy

The temperature-dependent dielectric properties of $Cu_{0.5}Co_{0.5}Fe_{2-x}La_xO_4$ (x = 0.16 and 0.20) ferrites were investigated at a constant frequency of 100 Hz in the temperature range of 30–400°C (Figure3).

Ianna Journal of Interdisciplinary Studies, EISSN: 2735-9891

Volume 7, Issue 2, 2025

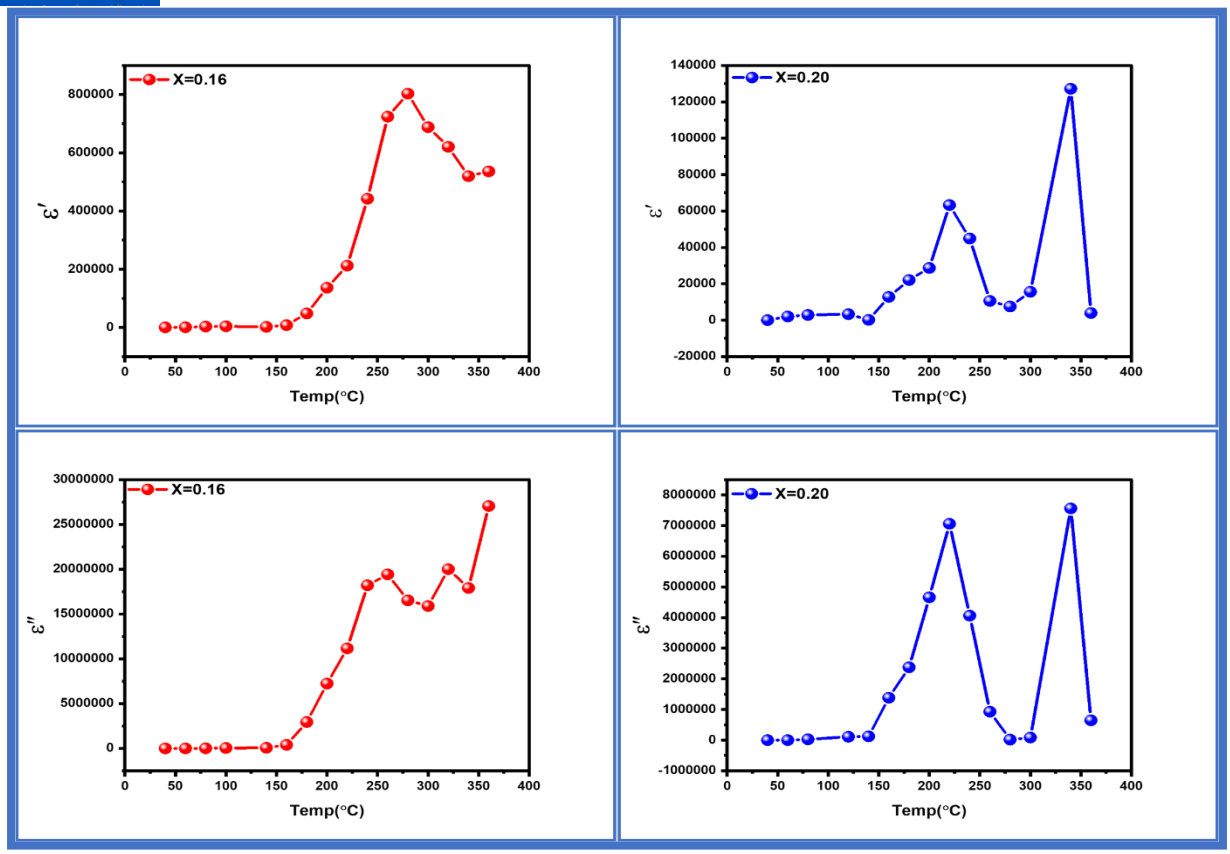

Figure 3: Temperature dependent dielectric constant (ε′) and the imaginary part (dielectric loss, ε″) of $Cu_{0.5}Co_{0.5}Fe_{2-x}La_xO_4$ (x = 0.16 and 0.20) spinel nanoferrite

Both the real part of the dielectric constant (ε′) and the imaginary part (dielectric loss, ε″),Eq(17)-Eq(18), exhibit strong temperature dependence for both composition(Table 6)

$$\varepsilon' = \frac{Ct}{\varepsilon_0 A} \tag{17}$$

$$\tan\delta = \frac{\varepsilon'}{\varepsilon''} \tag{18}$$

For x = 0.16, the dielectric constant (ε′) increases gradually at lower temperatures and rises sharply above 150°C, attaining an exceptionally high maximum value of approximately 1.1 × 10^6 around 290–310°C, corresponding to the ferroelectric-to-paraelectric transition (Curie temperature, Tc). Similarly, the dielectric loss (ε″) remains relatively low at lower temperatures but increases dramatically above 250°C, reaching a very high value of nearly 28–30 × 10^6 at elevated temperatures. In contrast, the sample with x = 0.20 shows significantly suppressed dielectric response: the maximum dielectric constant decreases to approximately 1.3 × 10^5 with the Curie temperature slightly shifted to a higher range (320–340°C), while the dielectric loss is reduced by nearly 75%, attaining a maximum of only 7–8 × 10^6.

Table 6. Temperature-dependent dielectric parameters of $Cu_{0.5}Co_{0.5}Fe_{2-x}La_xO_4$ (x = 0.16 and 0.20) ferrites at 100 Hz.

Parameter	Symbol	x = 0.16	x = 0.20	**Remark**
Maximum Dielectric Constant	ε'_{max}	~ 1.10×10^6	~ 1.30×10^5	~88% reduction
Maximum Dielectric Loss	ε''_{max}	~ $28 – 30 \times 10^6$	~ $7 – 8 \times 10^6$	~75% reduction
Curie Temperature	Tc	290 – 310 °C	320 – 340 °C	Slight increase
Frequency	f	100 Hz	100 Hz	Constant

This remarkable reduction in both ε′ and ε″ with increasing La^{3+} concentration is primarily attributed to the substitution of Fe^{3+} ions by stable La^{3+} ions at the octahedral [B] sites, which restricts the electron hopping between $Fe^{2+} \leftrightarrow Fe^{3+}$ and $Co^{2+} \leftrightarrow Co^{3+}$ ion pairs, thereby diminishing Maxwell-Wagner interfacial polarization and conduction losses. The rapid increase in both dielectric constant and loss at higher temperatures is due to the thermal activation of charge carriers, which enhances space charge polarization and hopping conduction. The slight increase in Curie temperature with La doping indicates improved thermal stability of the dielectric response, consistent with the enhanced crystallinity and reduced lattice strain observed in XRD analysis. Overall, these results demonstrate that La^{3+} substitution effectively tunes the dielectric behavior from giant dielectric constant/high loss (x = 0.16) to moderate dielectric constant/lower loss (x = 0.20), making these materials promising for tunable dielectric and microwave applications[30-33].

4.Conclusions

In conclusion, the substitution of La^{3+} ions in $Cu_{0.5}Co_{0.5}Fe_{2-x}La_xO_4$ spinel ferrites effectively modulates their structural, magnetic, and dielectric properties. XRD analysis confirmed the formation of a single-phase cubic spinel structure with improved crystallinity and marginal lattice expansion. Bertaut's intensity ratio method established the strong preference of La^{3+} for octahedral [B] sites.Magnetic studies demonstrated a sharp decline in saturation magnetization and net magnetic moment with increasing La^{3+} concentration, resulting from the dilution of magnetic Fe^{3+} ions and weakening of A–O–B superexchange interactions. Temperature-dependent dielectric spectroscopy at 100 Hz revealed a transition from giant dielectric constant/high loss behavior (x = 0.16) to significantly reduced dielectric constant and loss with slightly improved thermal stability (x = 0.20), as evidenced by the shift in Curie temperature toward higher values.

The strong interdependence observed among cation distribution, magnetic properties, and dielectric response underscores the efficacy of La^{3+} modulation in engineering the multifunctional characteristics of these ferrites. The tunable magnetic softness combined with controlled dielectric behavior positions these materials as promising candidates for microwave absorption, electromagnetic interference (EMI) shielding, high-frequency inductors, and dielectric devices. Further investigations on frequency-dependent properties in the microwave region are recommended to optimize their performance for practical applications.

Acknowledgements

The authors are grateful to the Sophisticated Test and Instrumentation Centre (STIC), Cochin, for providing X-ray Diffraction (XRD) facilities. We sincerely thank the Central Instruments Facility (CIF), Indian Institute of Technology Guwahati, for extending the Vibrating Sample Magnetometer (VSM) measurement facility. We also acknowledge the Department of Physics, Dr. Babasaheb Ambedkar

College, Nagpur, for providing the Wayne Kerr Precision Impedance Analyzer (Model 6500B) for temperature-dependent dielectric measurements.

References

[1], J., Zhao, B., Xiang, H., Dai, F., Liu, Y., Zhang, R., & Zhou, Y. (2022). High-entropy spinel ferrites MFe2O4 (M = Mg, Mn, Fe, Co, Ni, Cu, Zn) with tunable electromagnetic properties and strong microwave absorption. *Journal of Advanced Ceramics, 11*, 754 - 768. https://doi.org/10.1007/s40145-022-0569-3.

[2]Naz, K., Khan, J., Khalid, M., Akhtar, M., Gilani, Z., Asghar, H., Mersal, G., Ibrahim, M., Muhammad, A., & Ashiq, M. (2022). Structural, dielectric, impedance and electric modulus analysis of Ni substituted copper spinel ferrites nanoparticles for microwave device applications. *Materials Chemistry and Physics*. https://doi.org/10.1016/j.matchemphys.2022.126091.

[3]Salih, S., & Mahmood, W. (2023). Review on magnetic spinel ferrite (MFe2O4) nanoparticles: From synthesis to application. *Heliyon, 9*. https://doi.org/10.1016/j.heliyon.2023.e16601.

[4]Dastjerdi, D., Shokrollahi, H., & Mirshekari, S. (2023). A review of synthesis, characterization, and magnetic properties of soft spinel ferrites. *Inorganic Chemistry Communications*. https://doi.org/10.1016/j.inoche.2023.110797.

[5]Ansari, S., Younis, A., Kolekar, Y., & Ramana, C. (2025). Cobalt ferrite nanoparticles: The physics, synthesis, properties, and applications. *Applied Physics Reviews*. https://doi.org/10.1063/5.0244555.

[6]Aman, S., Alharbi, F., Gouadria, S., & Farid, H. (2023). Lanthanum substituted barium spinel ferrites, enhancement in various properties nanocrystalline ferrites. *Journal of Materials Science: Materials in Electronics, 34*, 1-8. https://doi.org/10.1007/s10854-023-09990-8.

[7]Alhadhrami, A., Zeshan, M., Muhammad, H., & Farid, T. (2023). The structural and dielectric properties of lanthanum substituted strontium based spinel ferrites nano-materials for high frequency device applications. *Journal of Taibah University for Science, 17*. https://doi.org/10.1080/16583655.2023.2236368.

[8]Routray, K., Saha, S., & Behera, D. (2019). Rare-earth (La3+) substitution induced changes in the structural, dielectric and magnetic properties of nano-CoFe2O4 for high-frequency and magneto-recording devices. *Applied Physics A, 125*, 1-15. https://doi.org/10.1007/s00339-019-2615-8.

[9]Abdo, M., Mansour, S., Al-Hazmi, F., AlHammad, M., & Sadeq, M. (2021). Enhancing the Magnetization, Dielectric Loss and Photocatalytic Activity of Co-cu Ferrite Nanoparticles Via the Substitution of Rare Earth Ions. *Journal of Materials Research and Technology*. https://doi.org/10.21203/rs.3.rs-770192/v1.

[10]Khan, M., Mahajan, H., & Srivastava, A. (2024). Investigation of Crystallographic, Morphological, Magnetic and Electrochemical Properties of La-Doped Cu-CoFe2O4 Spinel Ferrites. *Crystal Research and Technology, 59*. https://doi.org/10.1002/crat.202300356.

[11]Lin, Q., Yuan, G., He, Y., Wang, L., Dong, J., & Yu, Y. (2015). The influence of La-substituted Cu0.5Co0.5Fe2O4 nanoparticles on its structural and magnetic properties. *Materials & Design, 78*, 80-84. https://doi.org/10.1016/j.matdes.2015.04.029.

[12]Abdo, M., Mansour, S., Al-Hazmi, F., AlHammad, M., & Sadeq, M. (2021). Enhancing the Magnetization, Dielectric Loss and Photocatalytic Activity of Co-cu Ferrite Nanoparticles Via the

Substitution of Rare Earth Ions. *Journal of Materials Research and Technology*. https://doi.org/10.21203/rs.3.rs-770192/v1.

[13]Channagoudra, G., Nunez, J., Hadimani, R., & Dayal, V. (2022). Study of cation distribution in La3+ and Eu3+ substituted cobalt ferrite and its effect on magnetic properties. *Journal of Magnetism and Magnetic Materials*. https://doi.org/10.1016/j.jmmm.2022.169550.

[14]Khan, M., Mahajan, H., & Srivastava, A. (2024). Investigation of Crystallographic, Morphological, Magnetic and Electrochemical Properties of La-Doped Cu-CoFe2O4 Spinel Ferrites. *Crystal Research and Technology, 59*. https://doi.org/10.1002/crat.202300356.

[15]Channagoudra, G., Nunez, J., Hadimani, R., & Dayal, V. (2022). Study of cation distribution in La3+ and Eu3+ substituted cobalt ferrite and its effect on magnetic properties. *Journal of Magnetism and Magnetic Materials*. https://doi.org/10.1016/j.jmmm.2022.169550.

[16]Ikram, S., Arshad, M., Mahmood, K., Ali, A., Amin, N., & Ali, N. (2018). Structural, magnetic and dielectric study of La3+ substituted Cu0.8Cd0.2Fe2O4 ferrite nanoparticles synthesized by the co-precipitation method. *Journal of Alloys and Compounds*. https://doi.org/10.1016/j.jallcom.2018.08.065.

[17]Islam, M., Hossain, A., Ahsan, M., Bally, M., Ullah, M., Hoque, S., & Khan, F. (2022). Structural characteristics, cation distribution, and elastic properties of Cr3+ substituted stoichiometric and non-stoichiometric cobalt ferrites. *RSC Advances, 12*, 8502 - 8519. https://doi.org/10.1039/d1ra09090a.

[18]Shitole, R., Barote, V., Kadam, S., Kadam, S., Wadgane, S., Shinde, V., Hussain, S., Batoo, K., Shirsath, S., & Kadam, R. (2023). Williamson-Hall strain analysis, cation distribution and magnetic interactions in Dy3+ substituted zinc-chromium ferrite. *Journal of Magnetism and Magnetic Materials*. https://doi.org/10.1016/j.jmmm.2023.171468.

[19]Lakhani, V., Pathak, T., Vasoya, N., & Modi, K. (2011). Structural parameters and X-ray Debye temperature determination study on copper-ferrite-aluminates. *Solid State Sciences, 13*, 539-547. https://doi.org/10.1016/j.solidstatesciences.2010.12.023.

[20]Thanh, T., Nha, T., Giang, T., Nam, P., Toan, D., Khan, D., Manh, D., & Phong, P. (2024). Structural, optical, magnetic properties and energy-band structure of MFe2O4 (M = Co, Fe, Mn) nanoferrites prepared by co-precipitation technique. *RSC Advances, 14*, 23645 - 23660. https://doi.org/10.1039/d4ra04692g.

[21]Thi, N., Thanh, P., Arshad, M., Hasan, M., Akhtar, M., Dr, N., Mahmood, K., Trakoolwilaiwan, T., Kim, N., Thanh, P., Dr, N., Nicola, P., Morley, P., Sajjad, M., Rehman, A., Tung, L., & Thi, N. (2022). Structural, optical, electrical, dielectric, molecular vibrational and magnetic properties of La3+ doped Mg–Cd–Cu ferrites prepared by Co-precipitation technique. *Ceramics International*. https://doi.org/10.1016/j.ceramint.2022.01.313.

[22]Abdo, M., Mansour, S., Al-Hazmi, F., AlHammad, M., & Sadeq, M. (2021). Enhancing the Magnetization, Dielectric Loss and Photocatalytic Activity of Co-cu Ferrite Nanoparticles Via the Substitution of Rare Earth Ions. *Journal of Materials Research and Technology*. https://doi.org/10.21203/rs.3.rs-770192/v1.

[23]Kumar, L., & Kar, M. (2012). Effect of La3+ substitution on the structural and magnetocrystalline anisotropy of nanocrystalline cobalt ferrite (CoFe2−xLaxO4). *Ceramics International, 38*, 4771-4782. https://doi.org/10.1016/j.ceramint.2012.02.065.

[24]Kumar, L., & Kar, M. (2012). Effect of La3+ substitution on the structural and magnetocrystalline anisotropy of nanocrystalline cobalt ferrite (CoFe2−xLaxO4). *Ceramics International*, *38*, 4771-4782. https://doi.org/10.1016/j.ceramint.2012.02.065.

[25]Patil, B., Pawar, A., Bhosale, D., Ghodake, J., Thorat, J., & Shinde, T. (2019). Effect of La3+ substitution on structural and magnetic parameters of Ni–Cu–Zn nano-ferrites. *Journal of Nanostructure in Chemistry*, *9*, 119-128. https://doi.org/10.1007/s40097-019-0302-0.

[26]Khan, M., Mahajan, H., & Srivastava, A. (2024). Investigation of Crystallographic, Morphological, Magnetic and Electrochemical Properties of La-Doped Cu-CoFe2O4 Spinel Ferrites. *Crystal Research and Technology*, *59*. https://doi.org/10.1002/crat.202300356.

[27]Dasan, Y., Guan, B., Zahari, M., & Chuan, L. (2017). Influence of La3+ Substitution on Structure, Morphology and Magnetic Properties of Nanocrystalline Ni-Zn Ferrite. *PLoS ONE*, *12*. https://doi.org/10.1371/journal.pone.0170075.

[28]Channagoudra, G., Nunez, J., Hadimani, R., & Dayal, V. (2022). Study of cation distribution in La3+ and Eu3+ substituted cobalt ferrite and its effect on magnetic properties. *Journal of Magnetism and Magnetic Materials*. https://doi.org/10.1016/j.jmmm.2022.169550.

[29]Hameed, A., Asghar, A., Shabbir, S., Ahmed, I., Tareen, A., Khan, K., Hussain, G., Awaji, M., & Anwar, H. (2024). A detailed investigation of rare earth lanthanum substitution effects on the structural, morphological, vibrational, optical, dielectric and magnetic properties of Co-Zn spinel ferrites. *Frontiers in Chemistry*, *12*. https://doi.org/10.3389/fchem.2024.1433004.

[30]Kumar, P., Sharma, S., Knobel, M., & Singh, M. (2010). Effect of La3+ doping on the electric, dielectric and magnetic properties of cobalt ferrite processed by co-precipitation technique. *Journal of Alloys and Compounds*, *508*, 115-118. https://doi.org/10.1016/j.jallcom.2010.08.007.

[31]Kamran, M., & Anis-Ur-Rehman, M. (2022). Influence of La3+ substitutions on structural, dielectric and electrical properties of spinel cobalt ferrite. *Ceramics International*. https://doi.org/10.1016/j.ceramint.2022.10.127.

[32]Mugutkar, A., Gore, S., Tumberphale, U., Jadhav, V., Mane, R., Patange, S., Shaikh, S., Ubaidullah, M., Al-Enizi, A., & Jadhav, S. (2020). The role of La3+ substitution in modification of the magnetic and dielectric properties of the nanocrystalline Co-Zn ferrites. *Journal of Magnetism and Magnetic Materials*, *502*, 166490. https://doi.org/10.1016/j.jmmm.2020.166490.

[33]Phor, L., & Kumar, V. (2019). Structural, magnetic and dielectric properties of lanthanum substituted Mn0.5Zn0.5Fe2O4. *Ceramics International*. https://doi.org/10.1016/j.ceramint.2019.07.341.